Journal of Materials Chemistry

Cite this: J. Mater. Chem., 2011, 21, 18412

www.rsc.org/materials

PAPER

Phase transition, Raman spectra, infrared spectra, band gap and microwave dielectric properties of low temperature firing $(Na_{0.5x}Bi_{1-0.5x})(Mo_xV_{1-x})O_4$ solid solution ceramics with scheelite structures

Di Zhou,*[ab] Li-Xia Pang,[c] Hong Wang,[ab] Jing Guo,[ab] Xi Yao[ab] and Clive A. Randall[d]

Received 17th August 2011, Accepted 19th September 2011
DOI: 10.1039/c1jm14004c

A scheelite based structure that could host the solid solution $(Na_{0.5x}Bi_{1-0.5x})(Mo_xV_{1-x})O_4$ ($0.0 \leq x \leq 1.0$) was prepared *via* the solid state reaction method. All the compositions can be sintered well below a temperature of 800 °C. A structural phase transition occurs from the monoclinic scheelite structure to a tetragonal scheelite structure at $x = 0.10$ at room temperature. This structural transition is related to a displacive ferroelastic–paraelastic phase transition. This phase transition was also confirmed by *in situ* high temperature XRD and Raman studies, and a room temperature infrared spectra study. The compositions near the phase boundary possessed high dielectric permittivities (>70), and large *Qf* values (>80 000 GHz) with variable temperature coefficients of frequency and capacitance. For example, a temperature stable dielectric made as a composite with compositions of $x = 0.05$ and $x = 0.10$ was designed and co-sintered at 720 °C for 2 h to produce a dielectric with a permittivity of ~77.3, a *Qf* value between 8 000 GHz–10 000 GHz, and a temperature coefficient of <±20 ppm/°C at 3.8 GHz over a temperature range of 25–110 °C. This material is a candidate for dielectric resonators and low temperature co-fired ceramics technologies. Near the phase boundary at $x = 0.10$ in the monoclinic phase region, the samples show strong absorption in the visible light region and we determine a band gap energy of about 2.1 eV, which means that it might also be useful as a visible light irradiation photocatalyst.

I. Introduction

Microwave dielectric ceramics have been widely studied for more than forty years to meet the ever changing requirements for wireless applications, such as dielectric resonators, dielectric filters, dielectric antennas, *etc.* High performance microwave dielectric ceramics with a range of dielectric permittivities (ε_r) have been discovered and include materials, such as (Mg,Ca)TiO_3 for $\varepsilon_r \sim 20$, Ba(Mg,Zn,Sn,Ta,Nb)O_3 for $\varepsilon_r \sim 30$–40, (Zr,Sn)TiO_4 for $\varepsilon_r \sim 40$, (Sr,Ca)TiO_3–(La,Nd)AlO_3 for $\varepsilon_r \sim 45$, BaO–$(Sm,Nd)_2O_3$–TiO_2 for $\varepsilon_r \sim >70$. There is a need to expand the search for new microwave ceramics with either ultra-low permittivities (<5), ultra-high permittivities (>120) and ultra-low dielectric losses ($Q > 20\,000$).[1–6]

To achieve the miniaturization of microwave components for wireless communication, low temperature co-fired ceramic (LTCC) technology has become an important method due to its advantage in fabricating three-dimensional ceramic modules. The LTCC technology requires a lower sintering temperature of the ceramic than the melting point of the inner electrode material, besides the high dielectric performance.[7,8]

The scheelite structure with the typical composition ABO_4, belongs to the space group $I4_1/a$ (No. 88), and the nature of its structure provides flexibility for ion substitution on both A and B sites as described in Leight and Linn's work.[9] Microwave dielectric ceramics with scheelite/scheelite-related structures have been reported as an attractive structural family for these applications, for example compositions such as (Ca,Sr,Ba)(W,Mo)O_4, $BiVO_4$, $[(Li,Na,K,Rb,Ag)Bi]_{1/2}MoO_4$, and $[Li(Y,Yb)]_{1/2}WO_4$.[10–14] Among the scheelite structured ABO_4 compounds, $BiVO_4$ recently has attracted attention in a wide variety of applications, such as pigments, mixed (oxygen ionic–electronic) conductor materials, microwave dielectric materials, photocatalytic materials, *etc.*[15–20] $BiVO_4$ exists in three phases, monoclinic scheelite, tetragonal zircon and tetragonal scheelite.[21] The tetragonal zircon $BiVO_4$ can be synthesized by the precipitation method. When heated above 670–770 K, it irreversibly transforms into the monoclinic scheelite phase. The monoclinic

[a]*Electronic Materials Research Laboratory, Key Laboratory of the Ministry of Education, Xi'an Jiaotong University, Xi'an, 710049, China. E-mail: zhoudi1220@gmail.com; Fax: +862982668794; Tel: +862982668679*
[b]*International Center for Dielectric Research, Xi'an Jiaotong University, Xi'an, 710049, China*
[c]*Micro-optoelectronic Systems Laboratories, Xi'an Technological University, Xi'an, 710032, China*
[d]*The Pennsylvania State University, Center for Dielectric Studies, Materials Research Institute, University Park, PA, 16802, USA*

scheelite $BiVO_4$ can reversibly transition to the tetragonal scheelite phase by high temperature and applied external pressure, as reported by Bierlein *et al.*, David *et al.*, and Sleight *et al.*,[16,18,22] and *via* a second order ferroelastic phase transition. Among the three modifications of $BiVO_4$, the monoclinic scheelite phase shows photocatalytic oxidation of organic pollutants and has also been recognized as a strong photocatalyst for water splitting and pollutant decomposition under visible light irradiation.[23–25] Furthermore, it was reported to possess high performance microwave dielectric properties with $\varepsilon_r = 68$, $Qf = 6500$–8000 GHz, TCF = −243–−260 ppm/°C, and a sintering temperature below 900 °C,[13,20] which indicates that it might also be a candidate for low temperature co-fired ceramics (LTCC), the focus of this study.

An important way to modify the properties of materials is through compositional design in the form of solid solutions. In our previous work, $(Li_{0.5}Bi_{0.5})MoO_4$ was chosen as an end member to form a full range solid solution with $BiVO_4$, in which a number of novel phenomena were observed, including nonlinear change of cell parameters, phase transition, low sintering temperature, high quality microwave dielectric properties *etc.*[11,26] In the present work, the Na^+ and Mo^{6+} ions are chosen to substitute for the Bi^{3+} on the A site and V^{5+} on the B site. The full range of $(Na_{0.5x}Bi_{1-0.5x})(Mo_xV_{1-x})O_4$ ($0.0 \le x \le 1.0$) compositions (marked with NBMVx in the text) were prepared *via* the solid state reaction method. The phase composition, phase transition, microstructure, Raman spectra, infrared spectra, band gap energies, and microwave dielectric properties were all studied. Composite samples including the ferroelastic and paraelastic phases at room temperature were also designed to achieve more temperature stable microwave dielectric ceramics in a wide temperature range.

II. Experimental

Proportionate amounts of reagent-grade starting materials Bi_2O_3 (>99%, Shu-Du Powders Co. Ltd., Chengdu, China), Na_2CO_3 (>99%, Sinopharm Chemical Reagent Co., Ltd, Shanghai, China), MoO_3 (>99%, Fuchen Chemical Reagents, Tianjin, China) and V_2O_5 (>99%, Sinopharm Chemical Reagent Co., Ltd, Shanghai, China) were prepared according to the stoichiometric formulation $(Na_{0.5x}Bi_{1-0.5x})(Mo_xV_{1-x})O_4$. Powders were mixed and milled for 4 h using a planetary mill (Nanjing Machine Factory, Nanjing, China) by setting the running speed at 150 rpm with the zirconia balls (2 mm in diameter) as the milling medium. The powder mixture was then dried and calcined at 600–680 °C for 4 h according to the composition. The calcined powders were ball milled again for 5 h with a running speed of 200 rpm to obtain fine powders. Then powders were pressed into cylinders (12 mm in diameter and 5–6 mm in height) in a steel die with 5wt. % PVA binder addition under a uniaxial pressure of 200 MPa. The composite samples were pressed into cylinders from different granulated powders of NBMV0.05 and NBMV0.10 samples. Samples were sintered in the temperature range from 600 °C to 800 °C for 2 h. Room temperature XRD was performed using a XRD with CuKα radiation (Rigaku D/MAX-2400 X-ray diffractometry, Tokyo, Japan). High temperature XRD was performed in the temperature range from room temperature to 110 °C using a XRD with CuKα radiation (XRD-7000, Shimadzu, Kyoto, Japan). Prior to examination, sintered pellets were crushed in a mortar and pestle to powder. The diffraction pattern was obtained between 15–65° 2θ at a step size of 0.02°. To examine the grain morphology, as-fired surfaces were examined by scanning electron microscopy (SEM) (JSM-6460, JEOL, Tokyo, Japan). The Raman spectra at room temperature were obtained on polished pellets with a Raman spectrometer (inVia, Renishaw, England) excited by an Ar^+ laser (514.5 nm). The high temperature Raman spectra were measured using another Raman spectrometer (LabRAM HR800, HORIBA Jobin Yvon, France). The IR reflectivity spectra were measured using a Bruker IFS 66v FTIR spectrometer on an infrared beamline station (U4) at the National Synchrotron Radiation Lab. (NSRL), China. Dielectric behaviors at microwave frequency were measured with the $TE_{01\delta}$ dielectric resonator method with a network analyzer (HP 8720 Network Analyzer, Hewlett-Packard) and a temperature chamber (Delta 9023, Delta Design, Poway, CA). The temperature coefficient of the resonant frequency TCF (τ_f) was calculated with the following formula:

$$\mathrm{TCF}(\tau_f) = \frac{f_T - f_{T_0}}{f_{T_0} \times (T - T_0)} \times 10^6 \quad (1)$$

where f_T and f_{T_0} were the $TE_{01\delta}$ resonant frequencies at temperatures T and T_0, respectively.

III. Results and discussion

Phase and structure analysis by XRD and Raman spectroscopy

Fig. 1 shows the XRD patterns of $(Na_{0.5x}Bi_{1-0.5x})(Mo_xV_{1-x})O_4$ ceramics sintered at 680 °C for 2 h, and high temperature XRD patterns for the $x = 0.075$ sample measured in the temperature range 26–110 °C. As seen from Fig. 1(a), a full scheelite-like structure solid solution was obtained across the whole range $0.0 \le x \le 1.0$, which is consistent with the earlier work of Duraisamy and Ramanan.[27] When $x \ge 0.10$, the structure of $(Na_{0.5x}Bi_{1-0.5x})(Mo_xV_{1-x})O_4$ changes from the $BiVO_4$-type monoclinic distorted scheelite structure to a tetragonal scheelite structure. This is experimentally reflected in the data with the splitting of several reflection peaks, such as the (1 0 1) peak splitting into (1 0 1) and (0 1 1) peaks, the (2 0 0) peak splitting into (2 0 0) and (0 2 0) peaks *etc.* To check the temperature sensitivity of the phase transition in the $(Na_{0.5x}Bi_{1-0.5x})(Mo_xV_{1-x})O_4$ system, a high temperature XRD was performed on the sample at $x = 0.075$, which shows the monoclinic structure at room temperature, as shown in Fig. 1(b). The characteristic peak splitting was also observed in the high temperature XRD patterns of NBMV0.075 sample at around 60 °C. The cell parameters of a and b as a function of temperature are shown in Fig. 1(c). It is seen that a decreases and b increases with temperature almost linearly and they become closer and closer. At around 60 °C, the a and b become equal to each other, which means that the crystal structure changes from monoclinic to the tetragonal phase. The *in situ* XRD results give direct evidence of the phase transition in $(Na_{0.5x}Bi_{1-0.5x})(Mo_xV_{1-x})O_4$ system.

Schematic illustrations of the crystal structure of the scheelite ABO_4 phase and the network change of monoclinic and tetragonal structures along the *ab*-plane are shown in Fig. 2. The room temperature cell parameters, change in the cell parameter ratios

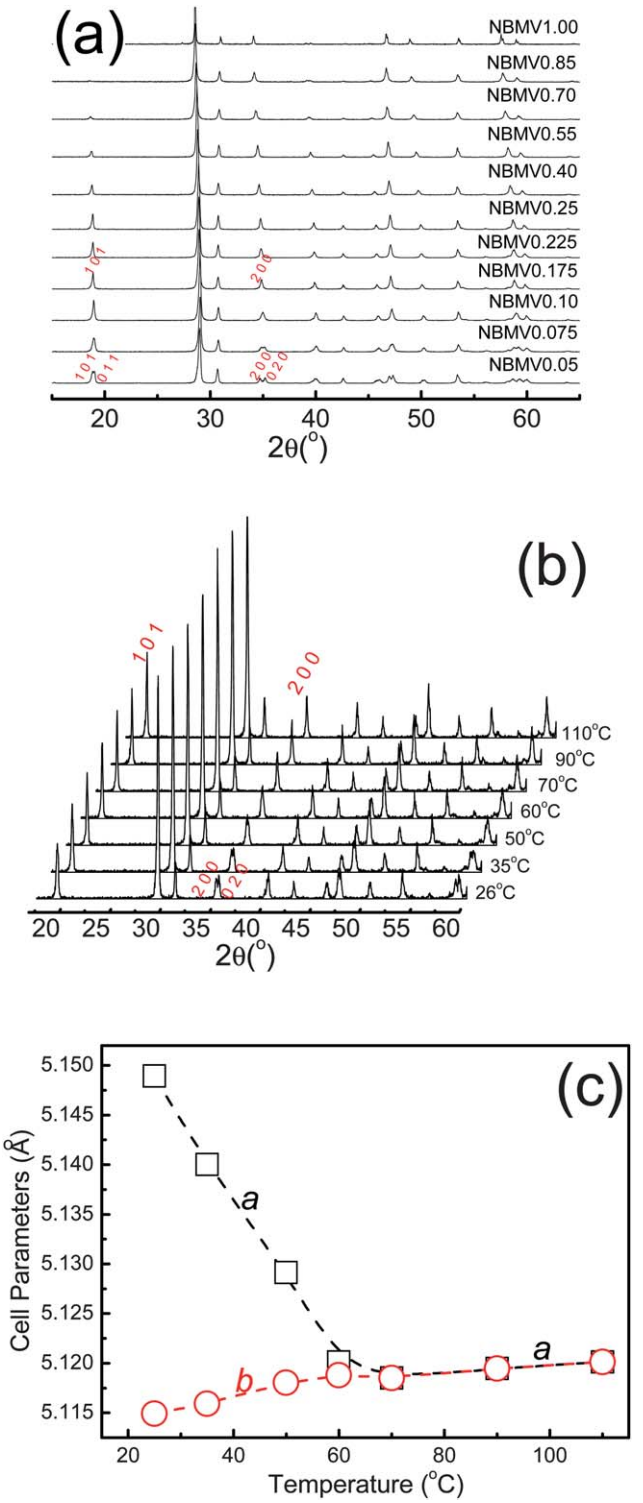

Fig. 1 (a) XRD patterns of $(Na_{0.5x}Bi_{1-0.5x})(Mo_xV_{1-x})O_4$ ceramics sintered at 680 °C for 2 h, (b) high temperature XRD patterns for a sample where $x = 0.075$, and (c) cell parameters a and b for the $x = 0.075$ sample as a function of temperature.

of a/c, b/c, atom volume and atom volume occupation of $(Na_{0.5x}Bi_{1-0.5x})(Mo_xV_{1-x})O_4$ ceramics as a function of the x value at room temperature of the whole $(Na_{0.5x}Bi_{1-0.5x})(Mo_xV_{1-x})O_4$ system are shown in Fig. 3 and Fig. 4. In the

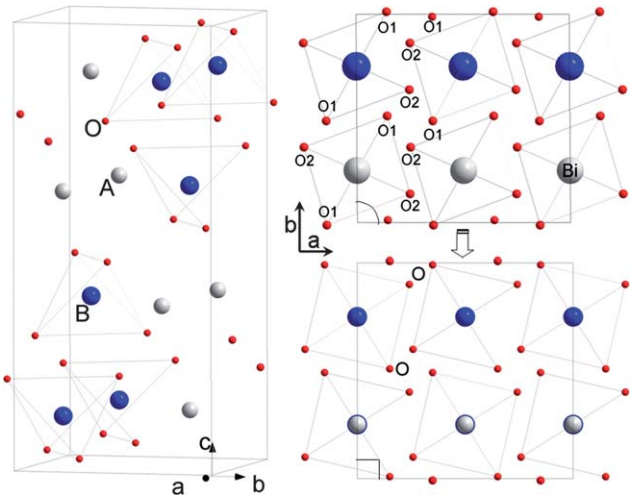

Fig. 2 Schematic illustrations of crystal structure of scheelite ABO_4 phase and the network change of monoclinic and tetragonal structures along the *ab*-plane.

ferroelastic monoclinic structure of ABO_4, the B–O_4 tetrahedra have two O anions at the top, further apart than those on the bottom, which are located in one tetrahedron and give one long B–O distance and a shorter one (as shown in Fig. 2, B–O_1 > B–O_2).[22] During the phase transition, the displacements of A and B are along the b axis; both cations move in the same direction[22] which results in an equal distance of B–O_1 = B–O_2. The displacements of the A-site Bi^{3+} cations were believed to play a major role in the transition, and the paraelastic phase lies midway between two permissible ferroelastic orientation states.[18] It is seen from Fig. 3 that the a and b parameters for the monoclinic structure ($x \leq 0.10$) are close to each other, about 5.10–5.20 Å, while the c parameter is about 11.7 Å. With the increase in the x value, the a parameter decreases, while the b and c parameters both decrease. At the phase boundary, $x = 0.1$, the a and b parameters become equal to each other and the β angle decreases from 90.35° to 90° for the tetragonal structure, corresponding to the merging of (1 0 1) and (0 1 1) into one peak, (2 0 0) and (0 2 0) into one peak, *etc.*, which were seen in the XRD

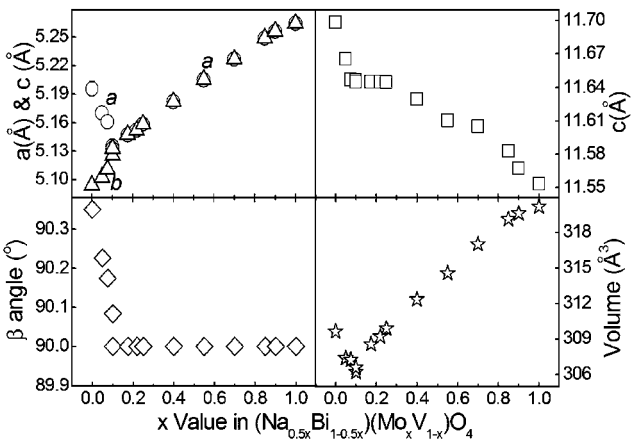

Fig. 3 Cell parameters and volume of $(Na_{0.5x}Bi_{1-0.5x})(Mo_xV_{1-x})O_4$ ceramics as a function of the x value at room temperature.

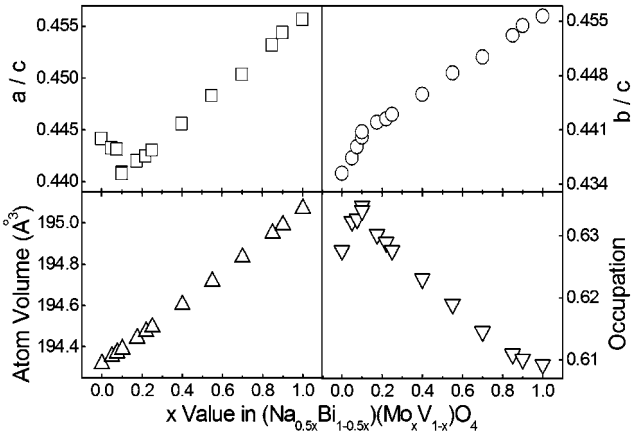

Fig. 4 Change of cell parameter ratios of *a*/*b*, *c*/*b*, atom volume and atom volume occupation of $(Na_{0.5x}Bi_{1-0.5x})(Mo_xV_{1-x})O_4$ ceramics as a function of the x value at room temperature.

patterns. A minimum cell volume value of about 306.2 Å^3 was obtained at the phase boundary, $x = 0.10$. When $x > 0.10$, the parameter a and cell volume V increase linearly, while the parameter b decreases linearly.

It is noticed that in $(Na_{0.5x}Bi_{1-0.5x})(Mo_xV_{1-x})O_4$ structure, the A-site is 8-fold coordinated, and the Bi^{3+} and Na^+ cations have radii of 1.17 Å and 1.18 Å, respectively. On the B-site which is 4-fold coordinated, V^{5+} and Mo^{6+} cations have radii of 0.355 Å and 0.41 Å, respectively, according to Shannon's data set.[28] Both the equivalent ionic radius $(1.17 + 0.005x)$ on the A site and $(0.355 + 0.055x)$ on the B site increase with the x value. The sum of the atom volume in a unit cell is $4 \times (V_A + V_B + 4 \times V_O)$ and increases linearly with the x value as shown in Fig. 4. Hence, it is understandable that the cell volume increases with the x value in the tetragonal phase region. However, in the monoclinic phase region, the cell volume decreases with the x value and reaches a minimum at $x = 0.1$. This implies that there is a build up of internal stress in the monoclinic phase. It is known that the pure monoclinic $BiVO_4$ can transition to the tetragonal phase by applied external pressure.[22] Here, the substitution of Na^+ and Mo^{6+} for Bi^{3+} and V^{5+}, on the A site and B site respectively, significantly increased the space occupancy and gave much internal pressure to the crystal structure of $(Na_{0.5x}Bi_{1-0.5x})(Mo_xV_{1-x})O_4$ ($x \leq 0.10$) to lead the crystal structure transition from monoclinic to tetragonal structure. A simple estimate of the internal stress, through the atomic volume occupation of the cell volume was calculated and is shown in Fig. 4. In the monoclinic phase region, the atom volume occupation increased linearly with the x value and reached a maximum value of about 63.5%.

Raman spectroscopy is often considered a very useful tool for determining the phase identification and also provides insight into the short-range character of the crystalline materials. Fig. 5 (a) shows the room-temperature Raman spectra of $(Na_{0.5x}Bi_{1-0.5x})(Mo_xV_{1-x})O_4$ ($0.0 \leq x \leq 1.0$) ceramics in the frequency range 100–1000 cm^{-1}. $BiVO_4$ has four chemical units in one unit cell and has a symmetry that is consistent with the *I*2/*a* space group. Through group theory and using irreducible representations, there are 15 different vibrational modes in $BiVO_4$, as follows:[29,30]

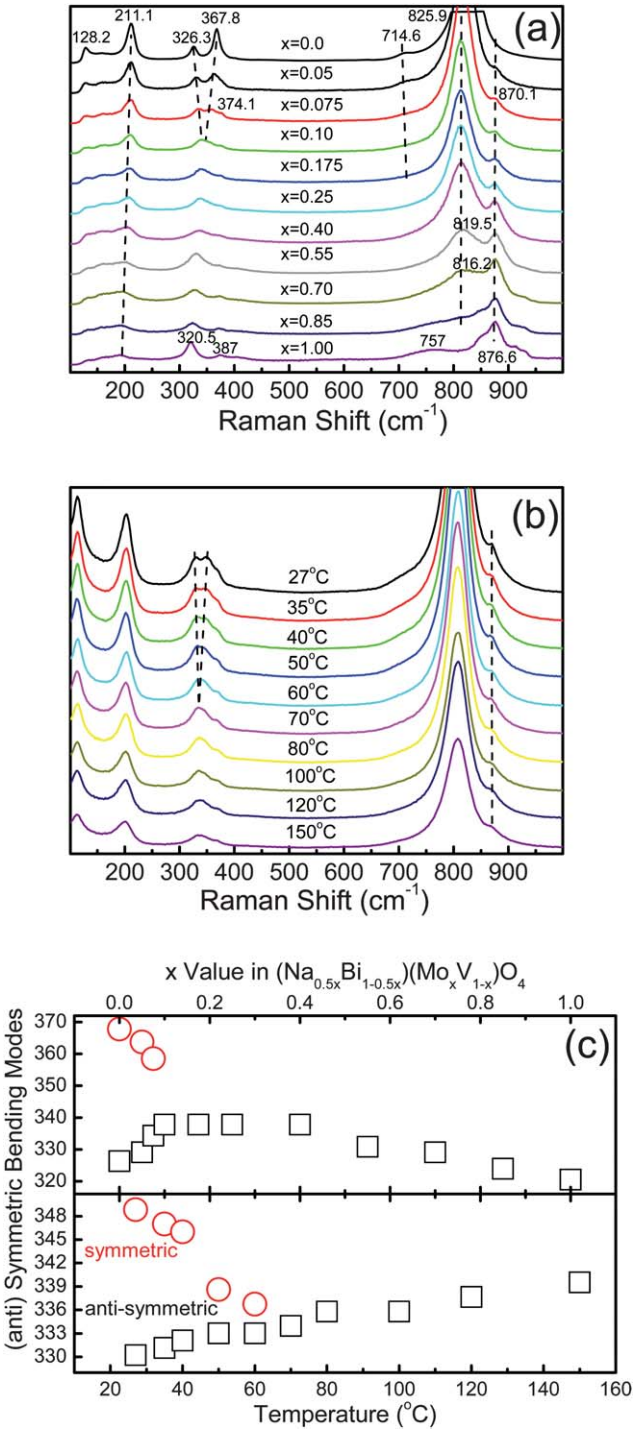

Fig. 5 (a) Room temperature Raman spectroscopy of the $(Na_{0.5x}Bi_{1-0.5x})(Mo_xV_{1-x})O_4$ ($0.0 \leq x \leq 1.0$) ceramics, (b) high temperature Raman spectroscopy for the sample $x = 0.075$ and (c) band shift for the (anti) symmetric bending mode as a function of temperature.

$$\Gamma = 3A_g + 2A_u + 6B_g + 4B_u \quad (2)$$

All g modes, A_g and B_g are Raman active; all u modes are IR active. It is seen that the spectra of $BiVO_4$ are dominated by an intense Raman band near 825.9cm^{-1} assigned to ν_s(V–O) (the

symmetric V–O stretching mode, A_g symmetry), and with a weak shoulder at about 714.6 cm^{-1} assigned to ν_{as}(V–O) (the anti-symmetric V–O stretching mode, B_g symmetry). The $\delta_s(VO_4^{3-})$ (the symmetric A_g bending mode of the vanadate anion) and $\delta_{as}(VO_4^{3-})$ (the anti-symmetric B_g bending mode of the vanadate anion) modes are near 367.8 and 326.3 cm^{-1}, respectively, and external modes (rotation/translation) occur near 211.1 cm^{-1} and 128.2 cm^{-1}, respectively. All results for the Raman peaks are in agreement with the literatures' reports.[30–35] It is seen that the most intensive modes ν_s(V–O) (A_g) gradually shift towards the low wave-number direction from 825.9 cm^{-1} for $BiVO_4$ to 816.2 cm^{-1} for NBMV0.70 as the x value increases from 0.00 to 0.70, revealing that the average short-range symmetry of the VO_4 tetrahedra becomes more regular,[30–34] whereas the full width at half maximum (FWHM) of the peak increases. It is known that Raman peak positions are sensitive to the short-range order and the Raman peak widths are more sensitive to the degree of crystallinity, defects, cation disorders, *etc.*[35] Therefore, the Raman results indicate that as the x value increases, the VO_4 tetrahedra become less symmetric, and the cation disorder increases. When x increased to 0.075, two extra bands are observed at 374.1 cm^{-1} and 870.1 cm^{-1}, which are assigned to the bending mode of molybdenum anion $\delta(MoO_4)$ and the Mo–O stretching mode, respectively. For the pure $(Na_{0.5}Bi_{0.5})MoO_4$, more Raman active modes (weak and overlapping) are observed than that of $BiVO_4$. The factor group analysis (FGA) predicts a total of 36 unit-cell modes, which are distributed among the following irreducible representations:

$$\Gamma = 3A_g + 5B_g + 5E_g + 5A_u + 3B_u + 5E_u \quad (3)$$

A_g, B_g and E_g modes are Raman active; A_u and E_u modes are IR active and B_u modes are inactive.[36–38] As seen in Fig. 5(a), the strongest mode is around 876.6 cm^{-1} and assigned to the $\nu_s(MoO_4)$ and the weaker mode near 757 cm^{-1} is assigned to $\nu_{as}(MoO_4)$. The Mo–O bending vibrations are localized in the 300–500 cm^{-1} region, in which the $\delta_s(MoO_4)$ mode is found at 320.5 cm^{-1} and the $\delta_{as}(MoO_4)$ mode is found at 387 cm^{-1}.[36–38] The short-range order and long-range disorder caused by the complex substitution of $(Na_{0.5}Bi_{0.5})$ on the A-site and Mo on the B-site in the scheelite structure lead to broadening and overlapping of Raman peaks. These results agreed well with Hanuza *et al.*'s work, in which it was deduced that the broadening of bands is due to the imperfect ordering of Bi^{3+} and Na^+ ions, which may be of the types Bi–Na–Bi–Na and Bi–Bi–Na–Na.[37] It is noticed that with the increase of the x value, the symmetric bending modes $\delta_s(VO_4^{3-})$ at 367.8 cm^{-1} redshifted and the anti-symmetric bending modes $\delta_{as}(VO_4^{3-})$ at 326.3 cm^{-1} blueshifted as shown in Fig. 5(c). When x reached 0.10, the symmetric bending modes $\delta_s(VO_4^{3-})$ and the anti-symmetric bending modes $\delta_{as}(VO_4^{3-})$ merged into one band, which is in accord with the structural change from monoclinic to the tetragonal phase, during which the lengths of the $V–O_1$ and $V–O_2$ bonds in the VO_4 tetrahedron (as shown in Fig. 2) become equal with each other. The *in situ* Raman spectra of the NBMV0.075 sample in the temperature range 27 °C–150 °C are shown in Fig. 5(b). As the temperature increases, the intensity of all the Raman bands decreases and the FWHM of the peak increases. The characteristic merging of the symmetric bending modes $\delta_s(VO_4^{3-})$ and the anti-symmetric bending modes $\delta_{as}(VO_4^{3-})$ was observed at around 60 °C. The detailed data are shown in Fig. 5(c) and have a similar trend to the situation in composition change. The *in* situ Raman results also give evidence for the phase transition in $(Na_{0.5x}Bi_{1-0.5x})(Mo_xV_{1-x})O_4$.

Microstructure and microwave dielectric properties

SEM micrographs of as-fired surfaces demonstrate the microstructure of the $(Na_{0.5x}Bi_{1-0.5x})(Mo_xV_{1-x})O_4$ ceramics ($x = 0.05$, 0.075, 0.175, 0.40, 0.55 and 0.70) sintered at different temperatures as shown in Fig. 6. Dense and homogeneous microstructures with almost no pores could be revealed in all compositions. It is seen that the grain size of $(Na_{0.5x}Bi_{1-0.5x})(Mo_xV_{1-x})O_4$ ceramics increased from 2–5 μm for the $x = 0.05$ sample to about 5–10 μm for the $x = 0.70$ sample although the sintering temperature was lowered by the substitution of Na^+ and Mo^{6+}.

Fig. 7 shows the microwave dielectric properties of $(Na_{0.5x}Bi_{1-0.5x})(Mo_xV_{1-x})O_4$ ($0.0 \le x \le 1.0$) ceramics as a function of the x value (at 3.5–6 GHz). The microwave permittivity of $(Na_{0.5x}Bi_{1-0.5x})(Mo_xV_{1-x})O_4$ ceramics increased linearly from 70 to 80 as the x value increased from 0.0 to 0.10 to a maximum in the monoclinic solid solution region, and then decreased down to 34.4 at the $(Na_{0.5}Bi_{0.5})MoO_4$ end member in the tetragonal solid solution region. The largest value of permittivity at the phase boundary might be attributed to the minimum cell volume, which means that the cell polarizability reached a maximum value. The Qf values increased approximately linearly from 9 500 GHz at $x = 0.0$ to 11 200 GHz at $x = 0.10$ and then decreased sharply to 4 300 GHz at $x = 0.25$. When the x value increases further, the Qf value increases and reaches 12 000 GHz for the end member $(Na_{0.5}Bi_{0.5})MoO_4$.

Generally speaking, the compositions near the phase boundary, such as $x = 0.05$, 0.075, 0.10, 0.175, possess high dielectric permittivity values and high Qf values. The only problem is the poor temperature dependence due to the phase transition. As shown in the Fig. 8(a), the NBMV0.05 sample is ferroelastic in the temperature range between 25–110 °C because of its high phase transition temperature above 110 °C. This determines that it has a large positive temperature coefficient of dielectric permittivity, 25–110 °C, which means a large negative TCF value. In contrast, the NBMV0.10's phase transition temperature lies at around 25 °C, and it has large negative temperature coefficient of dielectric permittivity at 25–110 °C, which means large positive TCF values. It must be noted that the dielectric permittivity of both NBMV0.05 and NBMV0.10 ceramics are almost linear with respect to the temperature dependence, not like the situation with the NBMV0.075, where the phase transition lies at around 68 °C, as shown in Fig. 8(a). Considering the XRD analysis above, all the results indicate that the ferroelastic–paraelastic phase transition temperature in the $(Na_{0.5x}Bi_{1-0.5x})(Mo_xV_{1-x})O_4$ ceramics was shifted from 255 °C for pure $BiVO_4$ to under room temperature for samples with $x \ge 0.10$. Although having poor temperature dependence of the dielectric permittivity, both NBMV0.05 and NBMV0.10 ceramics have high Qf values above 7 000 GHz and almost a linear temperature dependence of dielectric permittivity. This phenomenon provides a possibility to design a temperature stable composite sample with NBMV0.05 and NBMV0.10

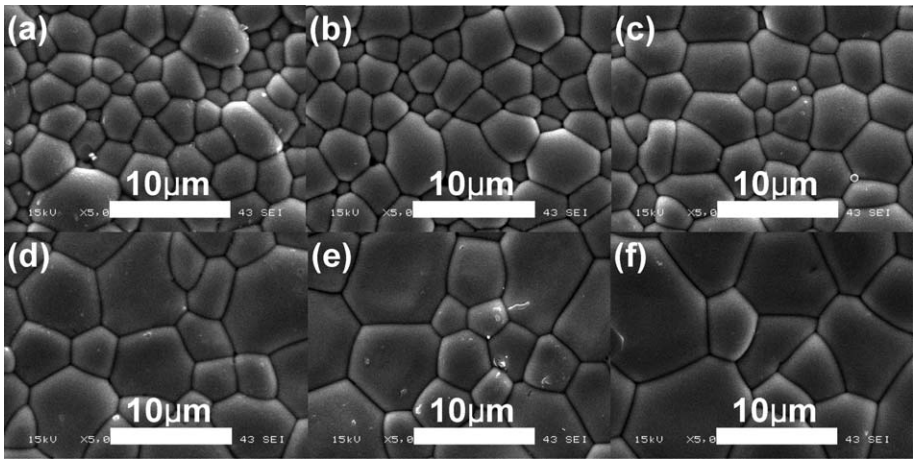

Fig. 6 SEM photos for (a) NBMV0.05 ceramics sintered at 760 °C for 2 h, (b) NBMV0.075 ceramic sintered at 760 °C for 2 h, (c) NBMV0.175 ceramic sintered at 720 °C for 2 h, (d) NBMV0.40 ceramic sintered at 700 °C for 2 h, (e) NBMV0.55 ceramic sintered at 700 °C for 2 h, and (f) NBMV0.70 ceramic sintered at 680 °C for 2 h.

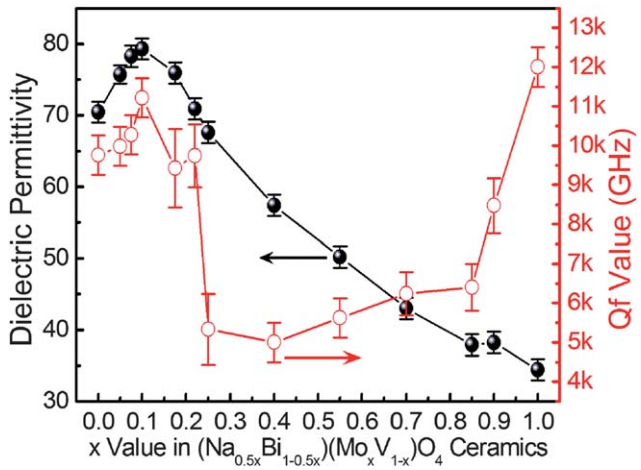

Fig. 7 Microwave dielectric permittivity, Qf value of the $(Na_{0.5x}Bi_{1-0.5x})(Mo_xV_{1-x})O_4$ ($0.0 \leq x \leq 1.0$) ceramics at room temperature as a function of the x value (at 3.5–6GHz).

compositions due to the opposite TCF values and similar sinterability. The microwave dielectric permittivity, Qf values and TCF values of composite samples as a function of temperature are shown in Fig. 8(weight ratio of NBMV0.05 to NBMV0.10 is 0.5, 0.57, 0.6 and 1.6 for NBMV1#, NBMV2#, NBMV3# and NBMV4#, respectively). It is seen that when the weight ratio of NBMV0.05 to NBMV0.10 is 0.6 : 1, the absolute values of TCF at 25–110 °C are smaller than 20 ppm/°C. The dielectric permittivity is stable at about 77.3 and the Qf value lies between 8 000 GHz–10 000 GHz at 25–110 °C for the temperature stable composite sample NBMV3# at 3.8 GHz. This system has comparable microwave dielectric performance with the traditional $BaO–Ln_2O_3–TiO_2$ (Ln = Sm, Nd *etc.*) system[6] but with a far lower sintering temperature. Besides the microwave resonator, filter applications, it might be also useful for the LTCC technology due to its low sintering temperature about 720 °C.

Infrared spectra and band gap study

Fig. 9 presents the IR reflectivity spectra of $(Na_{0.5x}Bi_{1-0.5x})(Mo_xV_{1-x})O_4$ ($0.0 \leq x \leq 1.0$) ceramics. It is seen that the two bands at 309.5 cm^{-1} and 357.2 cm^{-1}, which are assigned to the $\delta_{as}(VO_4)$ mode and the $\delta_s(VO_4)$ mode respectively, moved closer to each other with the increase in the x value and finally merged into one band at around $x = 0.10$. This is similar to the Raman analysis above and also supports the compositional phase transition at room temperature. The spectrum of $(Na_{0.5}Bi_{0.5})MoO_4$

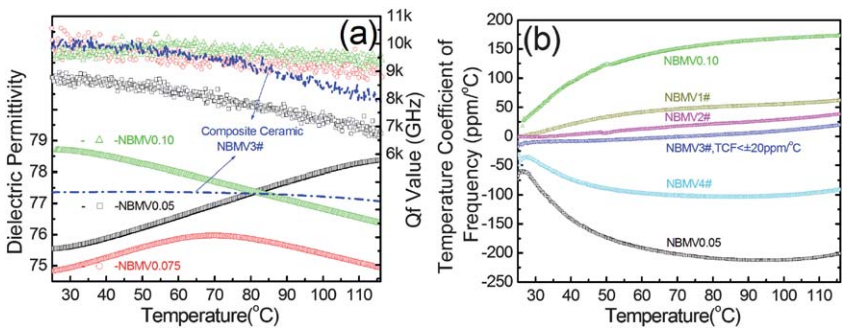

Fig. 8 (a) Microwave dielectric properties and (b) temperature coefficients of frequency as a function of temperature (in range 25–115 °C) of the $(Na_{0.5x}Bi_{1-0.5x})(Mo_xV_{1-x})O_4$ ceramics and composite samples sintered at 720 °C.

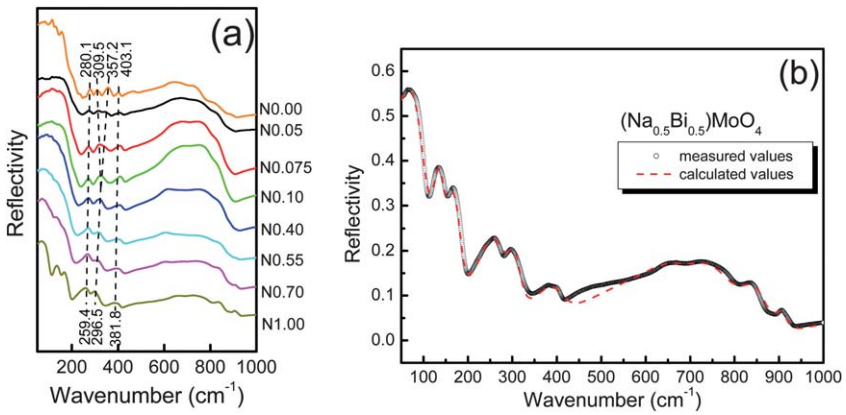

Fig. 9 (a) Infrared reflectivity spectra of the $(Na_{0.5x}Bi_{1-0.5x})(Mo_xV_{1-x})O_4$ ($0.0 \leq x \leq 1.0$) ceramics and (b) fitted values for pure $(Na_{0.5}Bi_{0.5})MoO_4$ ceramics.

was analyzed using a classical harmonic oscillator model. In this model the complex dielectric permittivity is written as:

$$\varepsilon^*(\omega) = \varepsilon_\infty + \sum_{j=1}^{n} \frac{\omega_{pj}^2}{\omega_{oj}^2 - \omega^2 - i\gamma_j\omega} \quad (4)$$

where $\varepsilon^*(\omega)$ is the complex dielectric function; ε_∞ is the dielectric constant caused by the electronic polarization at high frequencies; γ_j, ω_{oj} and ω_{pj} are the damping factor, the transverse frequency and oscillator strength of the j-th Lorentz oscillator, respectively; n is the number of transverse phonon modes. The complex reflectivity $R(\omega)$ can be written as:

$$R(\omega) = \left|\frac{1 - \sqrt{\varepsilon^*(\omega)}}{1 + \sqrt{\varepsilon^*(\omega)}}\right|^2 \quad (5)$$

The fitted result for pure $(Na_{0.5}Bi_{0.5})MoO_4$ is shown in Fig. 9 (b) and all the fitted parameters are listed in Table 1. It is noticed that the calculated permittivity of $(Na_{0.5}Bi_{0.5})MoO_4$ is 29.65 and a little smaller than the measured value of 34.4. It was concluded that the largest polarization contribution for the $(Na_{0.5}Bi_{0.5})MoO_4$ ceramic in the microwave region was attributed to the absorptions of phonon oscillation in the infrared region.

The optical absorption property of a semiconductor, which is relevant to the electronic structure feature, is recognized as the key factor in determining its photocatalytic activity.[39,40] As the x value increases, the color of samples becomes lighter and lighter from vivid yellow for pure $BiVO_4$ to a pale white for pure $(Na_{0.5}Bi_{0.5})MoO_4$. The grain size lies between 1–10 μm as studied above. The UV-vis diffuse reflectance spectra of $(Na_{0.5x}Bi_{1-0.5x})(Mo_xV_{1-x})O_4$ samples (x = 0.00, 0.10 and 1.00) are shown in Fig. 10(a). All the samples show strong absorption in the visible light region in addition to that in the UV region. The band gap absorption edge of pure $BiVO_4$ lies between 500–550 nm, which is similar to the literature reports. With the increase in the x value, the band gap absorption edge first redshifted to between 550–600 nm at $x = 0.10$ and then blueshifted to between 400–450 nm at $x = 1.00$. As a crystalline semiconductor, the optical absorption near the band edge follows the formula:[41]

$$\alpha h\nu = A(h\nu - E_g)^{n/2} \quad (6)$$

where α, ν, E_g and A are the absorption coefficient, light frequency, band gap energy and a constant, respectively. The n depends on the characteristics of the transition in a semiconductor, *i.e.* direct transition ($n = 1$) or indirect transition ($n = 4$). For $BiVO_4$, the value of n is 1.The energy of the band gap could be thus obtained from the plots of $(\alpha h\nu)^2$ *versus* photo energy ($h\nu$). (the detailed figures are not shown here) The calculated band gap energies of $(Na_{0.5x}Bi_{1-0.5x})(Mo_xV_{1-x})O_4$ samples as a function of x are shown in Fig. 10(b). The band gap energy of pure $BiVO_4$ was 2.35 eV and slightly smaller than the well-known value of 2.4 eV, which might be caused by the large grain sizes and defects of the ceramic sample.[42] As the x value increased, the band gap energy first sharply decreased to about 2.1 eV at around $x = 0.10$, and then increased non-linearly to about 3.02 eV for the other end member $(Na_{0.5}Bi_{0.5})MoO_4$ sample, which is also slightly smaller than the reported value of 3.1 eV.[43] For the whole $(Na_{0.5x}Bi_{1-0.5x})(Mo_xV_{1-x})O_4$ ($0.0 \leq x \leq 1.0$) system, the so-called bowing effect was taken into account and it was described by a second order equation as follows:[44,45]

$$E_g(x) = xE_g(A) + (1 - x)E_g(B) - bx(1 - x) \quad (7)$$

where E_g(A) and E_g(B) correspond to the band gap of the end member A and B, respectively. The parameter b is the optical bowing parameter, which is influenced by atomic size difference and chemical ionicity mismatch *etc.*[46] The observed nonlinearity

Table 1 Values of parameters derived from the fitting of the reflectivity spectra of $(Na_{0.5}Bi_{0.5})MoO_4$

Mode	ω_{oj}	ω_{pj}	γ_j	$\Delta\varepsilon_j$
1	65.92	305.92	50.24	21.51
2	132.76	154.98	30.21	1.36
3	164.77	148.17	33.84	0.809
4	258.88	257.8	69.204	0.992
5	302.19	148.11	37.384	0.24
6	397.44	219.59	83.733	0.305
7	663.99	392.47	141.2	0.349
8	747.26	495.97	139.89	0.441
9	842.26	282.18	75.579	0.112
10	907.11	120.54	30.146	0.018
$\varepsilon_\infty = 3.51$			$\varepsilon_0 = 29.65$	

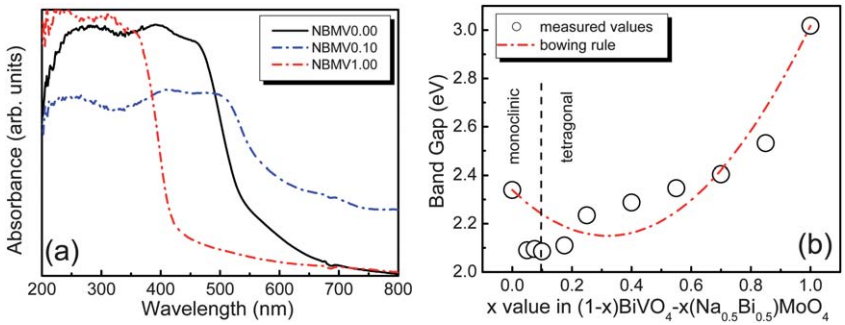

Fig. 10 (a) UV-vis diffuse reflectance spectra ($x = 0.00$, 0.10 and 1.00) and (b) band gap energy variation as a function of x in $(Na_{0.5x}Bi_{1-0.5x})(Mo_xV_{1-x})O_4$ solid solution ceramics.

in the band gap of $(Na_{0.5x}Bi_{1-0.5x})(Mo_xV_{1-x})O_4$ samples is fitted to eqn (7), yielding a small value for the bowing parameter b of 1.87 eV. In fact the fitting is not as good as the situations in pure semiconductors and simple oxide systems, such as III–V alloys, ZnO–CrO *etc.*[47,48] The band gap energy at around the phase boundary $x = 0.10$ was much smaller than the fitted values, while the tetragonal phase region has a slightly larger band gap energy than the fitted values. Apparently it looks like the minimum value of the second order curve shifted to the smaller band gap $BiVO_4$ end direction, which is similar to the results in CdO–CaO solid solution as reported by Srihari *et al.*[49] Lee *et al.* introduced a modified Vegard's law to explain the complex band gap compositional change trend in perovskite solutions (ABO_3) and it worked well.[50] However, the situation here is more complex and it was found that Vegard's law did not work well. Hence, no further comment or comparison is made on this issue. Anyway, the mismatch of the fitted and measured values here might be caused by the complex phase transition and cell parameter variation trend discussed above. As reported, although the scheelite monoclinic and tetragonal $BiVO_4$ have similar crystal structures and close band gap energies (2.4 eV for the monoclinic phase and 2.34 eV for the tetragonal phase).[15] the monoclinic $BiVO_4$ showed a much higher activity for photocatalytic O_2 evolution under visible light irradiation than tetragonal $BiVO_4$. Hence, the monoclinic solid solution in $(Na_{0.5x}Bi_{1-0.5x})(Mo_xV_{1-x})O_4$ with $0 < x \leq 0.10$ might be useful as a photocatalytic material for water splitting applications.

IV. Conclusions

In summary, a full scheelite-like solid solution was obtained in the $(Na_{0.5x}Bi_{1-0.5x})(Mo_xV_{1-x})O_4$ ($0.0 \leq x \leq 1.0$) ceramic and the phase boundary of the monoclinic and tetragonal phases lies at $x = 0.10$ at room temperature. The ferroelastic–paraelastic phase transition can also be induced by high temperature and this was confirmed by *in situ* high temperature XRD and Raman analysis. A temperature stable sample was obtained by co-firing a ferroelastic–paraelastic composite sample at 720 °C for 2 h, with a dielectric permittivity of 77.3, a high Qf value above 8 000 GHz and a small TCF value (<±20 ppm/°C) at 3.8 GHz in the temperature range 25–110 °C. Near the phase boundary at $x = 0.10$ in the monoclinic phase region, the samples show strong absorption in the visible light region with a band gap energy of about 2.1 eV. This system might be a candidate for microwave dielectric devices and LTCC technologies.

Acknowledgements

This work was supported by the National 973-project of China (2009CB623302), the Fundamental Research Funds for the Central University, National Project of International Science and Technology Collaboration (2009DFA51820), NSFC projects of China (60871044, 50835007), and the National Science Foundation I/UCRC program. The authors would like to thank Qiu-Ping Wang, Han-Chen Liu, Chao Zhou, Xiao-Hui Song, Yu-Yin Wang, Tao Shao and Ze-Ming Qi for their help in Raman, UV and IR experiments. The authors also thank the administrators in the IR beamline workstation of National Synchrotron Radiation Laboratory (NSRL) for their help in the IR measurements.

References

1 M. Mirsaneh, O. P. Leisten, B. Zalinska and I. M. Reaney, *Adv. Funct. Mater.*, 2008, **18**, 2293.
2 L. W. Chu, G. H. Hsiue and I. N. Lin, *Acta Mater.*, 2006, **54**, 1671.
3 R. I. Scotta, M. Thomas and C. Hampson, *J. Eur. Ceram. Soc.*, 2003, **23**, 2467.
4 S. Hirano, T. Hayashi and A. Hattori, *J. Am. Ceram. Soc.*, 1991, **74**, 1320.
5 B. Jancar, D. Suvorov, M. Valant and G. Drazic, *J. Eur. Ceram. Soc.*, 2003, **23**, 1391.
6 Y. J. Wu and X. M. Chen, *J. Eur. Ceram. Soc.*, 1999, **19**, 1123.
7 M. T. Sebastian, *Dielectric Materials for Wireless Communication*, 2008, Elsevier, Jordan Hill, Oxford OX2 8DP, UK.
8 M. T. Sebastian and H. Jantunen, *Int. Mater. Rev.*, 2008, **53**, 57.
9 A. W. Leight and W. J. Linn, *Ann. N. Y. Acad. Sci.*, 1976, **272**, 22.
10 G. K. Choi, J. R. Kim, S. H. Yoon and K. S. Hong, *J. Eur. Ceram. Soc.*, 2007, **27**, 3063.
11 D. Zhou, W. G. Qu, C. A. Randall, L. X. Pang, H. Wang, X. G. Wu, J. Guo, G. Q. Zhang, L. Shui, Q. P. Wang, H. C. Liu and X. Yao, *Acta Mater.*, 2011, **59**, 1502.
12 D. Zhou, C. A. Randall, L. X. Pang, H. Wang, J. Guo, G. Q. Zhang, Y. Wu, K. T. Guo, L. Shui and X. Yao, *Mater. Chem. Phys.*, 2011, **129**, 688.
13 M. Valant and D. Suvorov, *J. Am. Ceram. Soc.*, 2000, **83**, 2721.
14 J. S. Kim, J. C. Lee, C. I. Cheon and H. J. Kang, *Jpn. J. Appl. Phys.*, 2006, **45**, 7397.
15 T. Duraisamy and A. Ramanan, *Solid State Ionics*, 1999, **120**, 233.
16 J. D. Bierlein and A. W. Sleight, *Solid State Commun.*, 1975, **16**, 69.
17 G. S. Li, D. Q. Zhang and J. C. Yu, *Chem. Mater.*, 2008, **20**, 3983.
18 W. I. F. David, A. M. Glazer and A. W. Hewat, *Phase Transitions*, 1979, **1**, 155.

19 A. Pinczuk, B. Welber and F. H. Dacol, *Solid State Commun.*, 1979, **29**, 515.
20 S. H. Wee, D. W. Kim and S. I. Yoo, *J. Am. Ceram. Soc.*, 2004, **87**, 871.
21 A. Kudo, K. Omori and H. Kato, *J. Am. Chem. Soc.*, 1999, **121**, 11459.
22 A. W. Sleight, H. Y. Chen, A. Ferretti and D. E. Cox, *Mater. Res. Bull.*, 1979, **14**, 1571.
23 A. Kudo, K. Ueda, H. Kato and I. Mikami, *Catal. Lett.*, 1998, **53**, 229.
24 S. Kohtani, M. Koshiko, A. Kudo, K. Tokumura, Y. Ishigaki, A. Toriba, K. Hayakawa and R. Nakagaki, *Appl. Catal., B*, 2003, **46**, 573.
25 S. Kohtani, J. Hiro, N. Yamamoto, A. Kudo, K. Tokumura and R. Nakagaki, *Catal. Commun.*, 2005, **6**, 185.
26 D. Zhou, C. A. Randall, H. Wang, L. X. Pang and X. Yao, *J. Am. Ceram. Soc.*, 2010, **93**, 2147.
27 T. Duraisamy and A. Ramanan, *Solid State Ionics*, 1999, **120**, 233.
28 R. D. Shannon, *Acta Crystallogr., Sect. A: Cryst. Phys., Diffr., Theor. Gen. Crystallogr.*, 1976, **A32**, 751.
29 R. L. Frost, D. A. Henry, M. L. Weier and W. Martens, *J. Raman Spectrosc.*, 2006, **37**, 722.
30 M. S. Jang, H. L. Park, J. N. Kim, J. H. Ro and Y. H. Park, *Jpn. J. Appl. Phys.*, 1985, **24**, 506.
31 F. D. Hardcastle, I. E. Wachs, H. Eckert and D. A. Jefferson, *J. Solid State Chem.*, 1991, **90**, 194.
32 A. Zhang, J. Zhang, N. Cui, X. Tie, Y. An and L. Li, *J. Mol. Catal. A: Chem.*, 2009, **304**, 28.
33 J. Yu and A. Kudo, *Adv. Funct. Mater.*, 2006, **16**, 2163.
34 F. D. Hardcastle and I. E. Wachs, *J. Phys. Chem.*, 1991, **95**, 503.
35 H. M. Zhang, J. B. Liu, H. Wang, W. X. Zhang and H. Yan, *J. Nanopart. Res.*, 2008, **10**, 767.
36 N. Weinstock, H. Schulze and A. Muller, *J. Chem. Phys.*, 1973, **59**, 5063.
37 J. Hanuza, M. Maczka, L. Macalik and J. Maas, *J. Mol. Struct.*, 1994, **325**, 119.
38 V. N. Moiseenko, Yu. I. Bogatirjov, A. M. Jeryemenko and S. V. Akimov, *J. Raman Spectrosc.*, 2000, **31**, 539.
39 J. Tang, Z. Zou and J. Ye, *Angew. Chem., Int. Ed.*, 2004, **43**, 4463.
40 J. Tang, Z. Zou and J. Ye, *Chem. Mater.*, 2004, **16**, 1644.
41 M. A. Butler, *J. Appl. Phys.*, 1977, **48**, 1914.
42 L. Zhou, W. Z. Wang, S. W. Liu, L. S. Zhang, H. L. Xu and W. Zhu, *J. Mol. Catal. A: Chem.*, 2006, **252**, 120.
43 H. Kato, N. Matsudo and A. Kudo, *Chem. Lett.*, 2004, **33**, 1216.
44 J. E. Bernardand and A. Zunger, *Phys. Rev. B*, 1986, **34**, 5992.
45 J. E. Bernardand and A. Zunger, *Phys. Rev. B*, 1987, **36**, 3199.
46 H. L. Shiand and Y. Duan, *Eur. Phys. J. B*, 2008, **66**, 439.
47 G. P. Donati, R. Kaspi and K. J. Malloy, *J. Appl. Phys.*, 2003, **94**, 5814.
48 S. Adachi, *Properties of Semiconductor Alloys: Group-IV, III–V and II–VI Semiconductors*, Wiley, NewYork, 2009.
49 V. Srihari, V. Sridharan, S. Chandra, V. S. Sastry, H. K. Sahu and C. S. Sundar, *J. Appl. Phys.*, 2011, **109**, 013510.
50 S. Lee, R. D. Levi, W. G. Qu, S. C. Lee and C. A. Randall, *J. Appl. Phys.*, 2010, **107**, 023523.